ACS OMEGA

http://pubs.acs.org/journal/acsodf

Article

Energy Transfer in the 2_u ($^1D_2$) Ion-Pair State of I_2 by Inelastic Collisions with Noble Gas Atoms

Shoma Hoshino,* Oji Yamamoto,* and Koichi Tsukiyama*

Cite This: *ACS Omega* 2022, 7, 3605−3612

Read Online

ACCESS | Metrics & More | Article Recommendations

ABSTRACT: We investigated the energy transfer in the 2_u ($^1D_2$) ion-pair state of I_2 by collision with noble gas atoms, Ar, Kr, and Xe, using an optical−optical double resonance/fluorescence detection technique. By analyzing the temporal profiles of the emission from the laser-excited 2_u ($^1D_2$) state at various noble gas pressures, the quenching rate constants $k_{q,2_u}^{Rg}$ were determined to be $(4.55 \pm 0.42) \times 10^{-10}$, $(4.23 \pm 0.11) \times 10^{-10}$, and $(6.83 \pm 0.16) \times 10^{-10}$ cm^3 molecule^{-1} s^{-1} for quenching by Ar, Kr, and Xe, respectively. The 2_g ($^1D_2$) ion-pair state, lying in the vicinity of the 2_u ($^1D_2$) state, was identified as a destination state by collision with Ar and Kr. Collision with Xe provided a new reactive pathway forming the excimer XeI(B). The rate constants were determined to be $k_{q,2_u-2_g}^{Ar} = (9.61 \pm 0.63) \times 10^{-11}$ cm^3 molecule^{-1} s^{-1} and $k_{q,2_u-2_g}^{Kr} = (4.87 \pm 0.34) \times 10^{-11}$ cm^3 molecule^{-1} s^{-1} for the formation of the 2_g ($^1D_2$) state by collision with Ar and Kr, respectively, and $k_{q,2_u-XeI}^{Xe} = (6.55 \pm 0.19) \times 10^{-11}$ cm^3 molecule^{-1} s^{-1} for the formation of XeI(B). The collisional cross sections calculated from the quenching rate constants were considerably larger than the molecular size, owing to the harpoon mechanism.

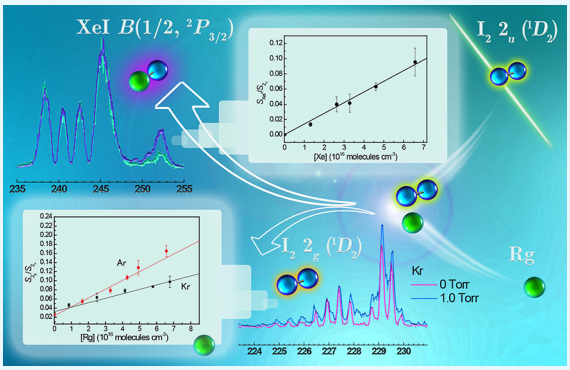

1. INTRODUCTION

The ion-pair states of halogen molecules are electronically excited charge-transfer states that correlate to positive and negative atomic ion pairs at the dissociation limits. In the I_2 molecule, a total of 20 ion-pair states are known, which are classified into four groups, or clusters, corresponding to the electronic states of I^+ ($^3P_2$, $^3P_{0,1}$, $^1D_2$, $^1S_0$) + I^- ($^1S_0$).[1] Spectroscopic investigations of the ion-pair states have been actively carried out along with the establishment of laser excitation techniques. In particular, the development of the perturbation-facilitated optical−optical double resonance method has greatly advanced the study of ion-pair states, in which the two-step excitation is performed with the lower valence state as the intermediate state enabled the quantum-state selective excitation of the ion-pair states with large equilibrium internuclear distances. The development of these experimental techniques has provided rich spectroscopic parameters of ion-pair states, and their spectral features have been clarified in detail. Notable characteristics are that ion-pair states belonging to the same group are located energetically close to each other and that they have a strongly bounded potential curve with a longer equilibrium internuclear distance than that of the valence states.[2]

Halogen molecules in the electronically excited states were known to exhibit a variety of curious radiative as well as nonradiative processes. For example, when the ICl molecule is excited to the A $^3\Pi_1$ state in the gas phase, it undergoes an addition reaction with acetylene. This property has been used for the isotope separation of ^{35}Cl and ^{37}Cl.[3,4] From our recent study on the ion-pair excited states of homonuclear halogen molecules,[5−8] we successfully identified the coexistence of an optical process called amplified spontaneous emission (ASE) with fluorescence. The generation of ASE between the excited states, so far reported on a few molecular systems like NO and NH_3, requires an inversion of population between the upper and lower states for light amplification, which, in turn, provided us with a unique way of controlling the population transfer between the relevant states through on/off of the population inversion.[9] As such, due to the coexistence of such novel processes with the rather classical behavior like spontaneous emission (fluorescence) and collisional energy transfer, the ion-pair states offer a benchmark for the dynamics in the charge-separated excited states. It is important to note here that the dynamic behavior sensitively depends on the individual ion-pair states, which

Received: November 4, 2021
Accepted: December 22, 2021
Published: January 14, 2022

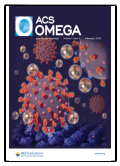

https://doi.org/10.1021/acsomega.1c06185
ACS Omega 2022, 7, 3605−3612

motivated the present state-to-state study in order to obtain a more detailed picture for the energy dissipation processes.

The collisional process of molecules with a change in quantum states before and after a collision is called inelastic collision, and many kinetic studies have been performed on such collisional processes. The collisional processes in the valence $B\ ^3\Pi(0_u^+)$ state of I_2 with various atomic and molecular quenchers have been studied extensively for many years. It is known that collisions in the $B\ ^3\Pi(0_u^+)$ state induce predissociation. For example, in the collisional process using noble gas atoms as quenchers, it has been confirmed that the rate constant of the collision-induced predissociation process increases as the vibrational quantum number increases.[10]

A non-adiabatic collisional process between ion-pair states of I_2 was first observed in 1924.[11] They suggested the highly efficient collisional transfer from the $D\ 0_u^+\ (^3P_2)$ state to the $D'\ 2_g\ (^3P_2)$ state, which was evidenced by the $D'\ 2_g\ (^3P_2) \rightarrow A'\ ^3\Pi(2_u)$ fluorescence at 342 nm after the $D\ 0_u^+\ (^3P_2)$ excitation. In this early study, however, the selective excitation of a single state was not possible due to the lack of energy resolution of the spectroscopic system. Therefore, the rate constants reported at that time were only averaged effective parameters. In ref 12, it was shown that the energy transfer from the $D\ 0_u^+\ (^3P_2)$ state to the $D'\ 2_g\ (^3P_2)$ state by collision with Ar was observed even at very low collisional energies. In the literature,[13] they reported that when the $D\ 0_u^+\ (^3P_2)$ state was generated in an Ar atmosphere at 100 Torr, the energy transfer was so efficient that the emission from the $D\ 0_u^+\ (^3P_2)$ state was hardly observed because of the rapid energy transfer from the $D\ 0_u^+\ (^3P_2)$ state to the $D'\ 2_g\ (^3P_2)$ state. The study of the collisions in a single rovibrational level of the ion-pair state was not possible until a more advanced laser excitation technique, such as the optical−optical double resonance method, became widespread.[14]

Regarding the self-quenching process in the ion-pair state of the I_2 molecule, Ubachs et al. first investigated the $E\ 0_g^+\ (^3P_2)$ state under single-collision conditions.[15] Since then, the collisional process between the $E\ 0_g^+\ (^3P_2)$ and $D\ 0_u^+\ (^3P_2)$ states has been investigated in detail by Akopyan et al.[16] and Fecko et al.[17,18] In the second tier ion-pair states, the collisional process between the $f\ 0_g^+\ (^3P_0)$ and $F\ 0_u^+\ (^3P_0)$ states was found, and the vibrational distributions were evaluated.[19,20] It has been explained both theoretically and experimentally that the vibrational distribution in the products due to collision-induced energy transfer depends on the energy gap between the initial and final states as well as on the magnitude of the Franck−Condon factor. We investigated the self-quenching processes in the $2_u\ (^1D_2)$ state in the third tier ion-pair states. In this experiment, the production of the $2_g\ (^1D_2)$ state, which was energetically located above the laser-prepared $2_u\ (^1D_2)$ state, was identified. Interestingly, for each vibrational level ($v_{2_u} = 3-7$) in the $2_u\ (^1D_2)$ state, vibrational levels with large Frank−Condon factors between the $2_u\ (^1D_2)$ and $2_g\ (^1D_2)$ states are generated. The large collisional cross sections calculated from the self-quenching rate constants are explained by the harpoon mechanism. The rate constant of the collision-induced energy-transfer process between the $2_u\ (^1D_2)$ and $2_g\ (^1D_2)$ states was found to be ∼15% of the total collisional process in the $2_u\ (^1D_2)$ state.[21]

In addition to the self-quenching process, studies on collisional processes using various simple molecules as collisional partners have been performed. In the collisional process of the $E\ 0_g^+\ (^3P_2)$ state with I_2, N_2, and CF_4 as collision partners, Akopyan et al. determined the reaction rate constants and the rovibrational distributions in the products by measuring the ratios of the $D\ 0_u^+\ (^3P_2) \rightarrow X\ ^1\Sigma_g^+$ and the $E\ 0_g^+\ (^3P_2) \rightarrow B\ ^3\Pi(0_u^+)$ emission intensities under various pressures.[22]

Several studies on the collisional and reaction processes in the ion-pair states of I_2 molecules with noble gas atoms have been conducted. Akopyan et al. investigated the collisional process of $E\ 0_g^+\ (^3P_2)$ and $D\ 0_u^+\ (^3P_2)$ states in the first tier and the $f\ 0_g^+\ (^3P_0)$ state in the second tier with He, Ar, Kr, and Xe.[23−25] Similar to the self-quenching process, transitions between the ion-pair states correlated to the same dissociation limit are observed primarily. However, the behavior for the first tier was different from that of the second tier. For example, in the first tier, the products are distributed in various electronic states of the same tier, whereas in the second tier, only energy transfer from the $f\ 0_g^+\ (^3P_0)$ state to the $F\ 0_u^+\ (^3P_0)$ states was recognized. Clarifying such differences in each tier would aid in understanding the nature of collisional energy relaxation in ion-pair states.

In the present study, we investigated the collisional process of the $2_u\ (^1D_2)$ state in the third tier with noble gas atoms, Ar, Kr, and Xe. Selective excitation of $2_u\ (^1D_2)$ ($v = 3$, $J = 23$) was performed using the optical−optical double-resonance method. The fluorescence at 247 nm from the initial $2_u\ (^1D_2)$ single state was detected, and the temporal profiles were measured under various noble gas pressures. The quenching rate constants were calculated for each noble gas atom from the Stern−Volmer plots, and the collisional mechanism was discussed based on these values. Assuming that the collision between the excited iodine and noble gas atoms is due to the harpoon mechanism, the theoretical rate constants calculated by a simple model are compared with the experimental values. From the emission spectra obtained from the excitation of the $2_u\ (^1D_2)$ state, it was found that the energy transfer between the $2_u\ (^1D_2)$ and $2_g\ (^1D_2)$ states is dominant in the case of Ar and Kr, while the reactive process of the XeI(B) formation is dominant in the collisional process with Xe. By determining the rate constants of these processes, we report new insights into the collisional processes in the high-energy states of I_2.

2. RESULTS AND DISCUSSION

2.1. Temporal Profile and UV Fluorescence Spectra from the $2_u\ (^1D_2)$ Ion-Pair State. Figure 1 shows the temporal

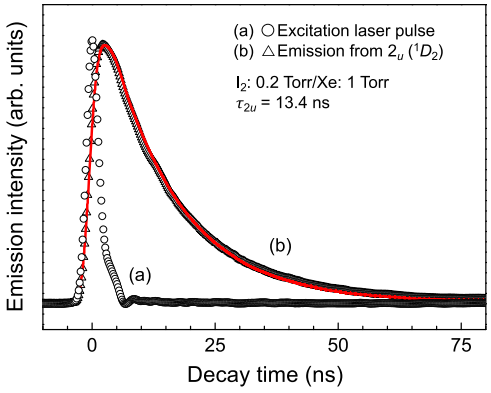

Figure 1. Temporal profiles of the (a) excitation laser pulse and (b) emission from the $2_u\ (^1D_2)$ ($v = 3$) state. The sample pressure; $p(I_2)$ = 0.2 Torr and $p(Xe)$ = 1.0 Torr. The temporal profile of the measured fluorescence (b: open triangle) can be fitted by a convoluted waveform of the temporal profile of the excitation laser (a). The best fit is shown by the red curve.

https://doi.org/10.1021/acsomega.1c06185
ACS Omega 2022, 7, 3605−3612

profiles of the excitation laser (circle) and the fluorescence at 247 nm (triangle) belonging to the transition from the 2_u ($^1D_2$) ($v = 3$, $J = 23$) ion-pair state to the $^3\Pi(2_g)$ valence state, where sample pressures were $p(I_2) = 0.2$ Torr and $p(Xe) = 1.0$ Torr, respectively. The temporal profile of the measured fluorescence can be fitted by a convoluted waveform of the temporal profile of the excitation laser and a single exponential decay function with decay time τ as follows

$$F(t) = C\int_0^t P(t')\exp[(t'-t)/\tau]dt' \quad (1)$$

where C and $P(t')$ are pre-exponential factors for adjusting the intensity and temporal profile of the excitation laser pulse.[26,27] Least-squares fitting was performed to determine decay lifetime τ. The convoluted waveform (solid red line in Figure 1), showing a satisfactory agreement with the observed temporal profile, corresponds to a decay time of $\tau = 13.4$ ns.

The temporal profile of the fluorescence from the 2_u ($^1D_2$) state is expressed by a kinetic model that considers the following processes

$$I_2(c\ ^1\Pi_g) + h\nu \rightarrow I_2(2_u) \quad (2)$$

$$I_2(2_u) \rightarrow I_2(\text{valence}) + h\nu\text{: } k_{R,2_u} \quad (3)$$

$$I_2(2_u) + I_2(X) \rightarrow \text{products: } k_{q,2_u}^{I_2} \quad (4)$$

$$I_2(2_u) + Rg \rightarrow \text{products: } k_{q,2_u}^{Rg} \quad (5)$$

By considering the competition of these processes, the inverse of the decay lifetime ($1/\tau$) can be expressed by the Stern–Volmer equation as

$$\frac{1}{\tau} = k_{R,2_u} + k_{q,2_u}^{I_2}[I_2(X)] + k_{q,2_u}^{Rg}[Rg] \quad (6)$$

The decay lifetimes were measured under various noble gas pressures, and the rate constants of the total collisional decay of the 2_u ($^1D_2$) ($v = 3$) state are determined to be $k_{q,2_u}^{Ar} = (4.55 \pm 0.42) \times 10^{-10}$ cm^3 molecule^{-1} s^{-1} for Ar, $k_{q,2_u}^{Kr} = (4.23 \pm 0.11) \times 10^{-10}$ cm^3 molecule^{-1} s^{-1} for Kr, and $k_{q,2_u}^{Xe} = (6.83 \pm 0.16) \times 10^{-10}$ cm^3 molecule^{-1} s^{-1} for Xe, from the Stern–Volmer plots as shown in Figure 2. The intercepts of each plot are within the range of the experimental error, which corresponds to the reciprocal of the fluorescence lifetime of the 2_u ($^1D_2$) ($v = 3$) state under the vapor pressure (0.2 Torr) of I_2. From our previously reported fluorescence lifetime τ_0 ($=1/k_{R,2_u}$) = (21.3 ± 0.1) ns and the self-quenching constant $k_{q,2_u}^{I_2} = (1.30 \pm 0.01) \times 10^{-9}$ cm^3 molecule^{-1} s^{-1} for the 2_u ($^1D_2$) ($v = 3$) state,[21] the inverse of the lifetime, $1/\tau$, at $p(I_2) = 0.2$ Torr is calculated to be $(5.54 \pm 0.03) \times 10^7$ s^{-1}. This value agrees with the intercepts shown in Figure 2 within the range of experimental error.

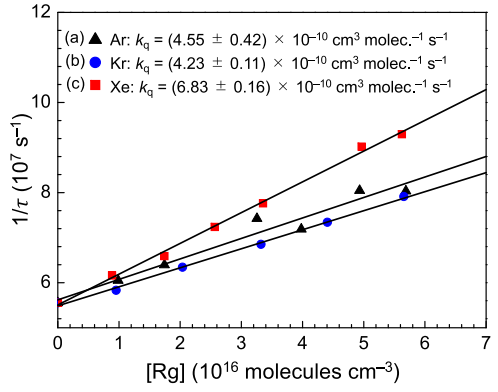

Figure 2. Stern–Volmer plot for the 2_u ($^1D_2$) ($v = 3$) state. Quencher; black triangle (a): Ar, blue circle (b): Kr, and red square (c): Xe.

Figure 3 shows the dispersed fluorescence spectra of the emission from the 2_u ($^1D_2$) ($v = 3$, $J = 23$) state with Xe, Kr, and Ar (top panel: pure vapor I_2, second: I_2 with Xe 1.0 Torr, third: I_2 with Kr 1.5 Torr, bottom: I_2 with Ar 1.5 Torr). The dispersed fluorescence spectrum of the pure I_2 sample consists of three band systems attributed to the 2_g ($^1D_2$)–A' $^3\Pi(2_u)$, 2_u ($^1D_2$)–$^3\Pi(2_g)$, and 2_u ($^1D_2$)–$^1\Delta(2_g)$ transitions from the shorter wavelength side. The 2_g ($^1D_2$) state, lying energetically adjacent to the laser-prepared 2_u ($^1D_2$) state, was generated by the same self-quenching process as in ref 21

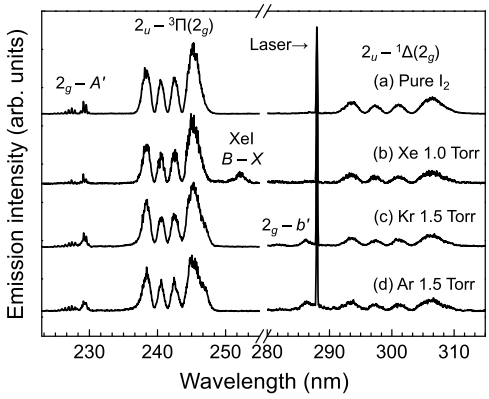

Figure 3. Dispersed fluorescence spectra obtained by the excitation of the 2_u ($^1D_2$) ($v = 3$) state. (a) Pure I_2 sample, (b) I_2 + Xe (1.0 Torr), (c) I_2 + Kr (1.5 Torr), and (d) I_2 + Ar (1.5 Torr).

$$I_2(2_u) + I_2(X) \rightleftarrows I_2(2_g) + I_2(X)\text{: } k_{q,2_u-2_g}^{I_2(X)} \quad (7)$$

In the case of Kr and Ar inclusions, in addition to the emission bands, a weak emission system attributable to the 2_g ($^1D_2$)–b' $^3\Delta(2_u)$ transition was observed at 285–290 nm. The intensities of these two emission systems from 2_g ($^1D_2$) at 220–230 and 285–290 nm were found to increase compared with those from 2_u ($^1D_2$) with increasing inserted noble gas pressures through the following quenching process

$$I_2(2_u) + Rg \rightleftarrows I_2(2_g) + Rg\text{: } k_{q,2_u-2_g}^{Rg} \quad (8)$$

We assume that the rate constants for the forward and reverse reactions in eqs 7 and 8 are equal.

In the case of Xe, only a slight increase in the fluorescence intensity was observed. Instead, the following reactive process was identified

$$I_2(2_u) + Xe \rightleftarrows XeI(B) + I\text{: } k_{q,2_u-XeI}^{Xe} \quad (9)$$

Again, as in processes 7 and 8, the rate constants for the forward and reverse reactions were assumed to be equal in the later analysis. When Xe is encapsulated, the emission around 253 nm is observed and assigned to the B ($1/2\ ^2P_{3/2}$) → X ($1/2\ ^2\Sigma^+$) transition of the XeI excimer produced by the process 9. A similar trend has been reported in previous studies on collision-induced processes in other ion-pair states.[25]

https://doi.org/10.1021/acsomega.1c06185
ACS Omega 2022, 7, 3605−3612

Figure 4 shows the temporal profiles obtained by monitoring the emission from the 2_u ($^1D_2$) state at 247 nm (triangle) and the

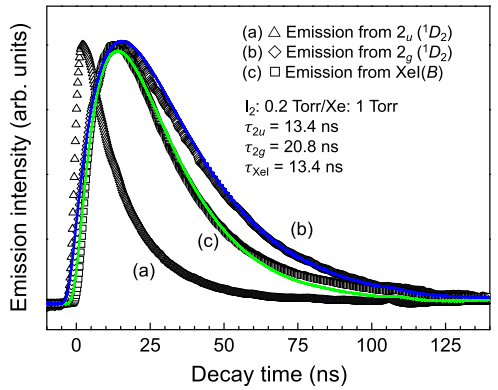

Figure 4. Temporal profiles of emission from the (a) 2_u ($^1D_2$) ($v = 3$) state, (b) 2_g ($^1D_2$) state of I_2, and (c) B ($1/2\ ^2P_{3/2}$) state of XeI. Sample pressure: $p(I_2)$ = 0.2 Torr and p(Xe) = 1.0 Torr. Waveforms (b: open rhombus) and (c: open square) can be fitted by a convoluted waveform of waveform (a). The best fit is shown by blue and green curves, respectively.

2_g ($^1D_2$) state at 230 nm (rhombus) of I_2 and the B ($1/2\ ^2P_{3/2}$) state of XeI at 253 nm (square) under p(Xe) = 1.0 Torr. The temporal profiles of the emission from the 2_g ($^1D_2$) and XeI(B) states can be reproduced by the convolved curve of the temporal profiles of the emission from the 2_u ($^1D_2$) state, assuming a single exponential decay function. This indicates that the temporal profile of the emission from the 2_u ($^1D_2$) state acts as the excitation function of those from the 2_g ($^1D_2$) state of I_2 and B ($1/2\ ^2P_{3/2}$) state of XeI, which are generated by the first-order process from the 2_u ($^1D_2$) state by collisions with iodine molecules in the 2_u ($^1D_2$) state. The decay time of the B ($1/2\ ^2P_{3/2}$) state of XeI was evaluated from the temporal analysis to be 13.4 ns, which concurs with the reported lifetime of the B ($1/2\ ^2P_{3/2}$) state, ~15 ns.[28]

2.2. Rate Constants for the Collision-Induced 2_u ($^1D_2$)–2_g ($^1D_2$) Transition. The rate constants for the formation of the 2_g ($^1D_2$) state indicated in reaction 8 were then determined. In addition to reactions 7 and 8, the fluorescence relaxation of the 2_g ($^1D_2$) state was considered as

$$I_2(2_g) \rightarrow I_2(\text{valence}) + h\nu\text{: } k_{R,2_g} \tag{10}$$

The net production rate of $I_2(2_g)$ is described as

$$\frac{dN_{2_g}(t)}{dt} = k_{q,2_u-2_g}^{Rg} N_{2_u}(t)[Rg] - k_{q,2_u-2_g}^{Rg} N_{2_g}(t)[Rg] + k_{q,2_u-2_g}^{I_2(X)} N_{2_u}(t)[I_2(X)] - k_{q,2_u-2_g}^{I_2(X)} N_{2_g}(t)[I_2(X)] - k_{R,2_g} N_{2_g}(t) \tag{11}$$

In the right-hand side of eq 11, the first and third terms correspond to the dissipation of the laser-prepared 2_u ($^1D_2$) state, the second and fourth terms to the dissipation of the 2_g ($^1D_2$) state by collisions, and the fifth term to the fluorescence decay of the 2_g ($^1D_2$) state. Here, the emission intensity $I_i(t)$ from the i state at time t can be expressed as $I_i(t) = k_{R,i} N_i(t)$ using the number density $N_i(t)$ and the radiative decay constant $k_{R,i}$. From this relationship, the rate eq 11 can be transformed as

$$\frac{dI_{2_g}(t)}{dt} = \frac{k_{R,2_g}}{k_{R,2_u}} k_{q,2_u-2_g}^{Rg}[Rg] I_{2_u}(t) - k_{q,2_u-2_g}^{Rg}[Rg] I_{2_g}(t) + \frac{k_{R,2_g}}{k_{R,2_u}} k_{q,2_u-2_g}^{I_2(X)}[I_2(X)] I_{2_u}(t) - k_{q,2_u-2_g}^{I_2(X)}[I_2(X)] I_{2_g}(t) - k_{R,2_g} I_{2_g}(t) \tag{12}$$

By integrating both sides of eq 12 from $t = 0$ to $t \rightarrow \infty$, we obtain the relation,

$$I_{2_g}(t \rightarrow \infty) - I_{2_u}(t=0) = \frac{k_{R,2_g}}{k_{R,2_u}} k_{q,2_u-2_g}^{Rg}[Rg] \int_0^\infty I_{2_u}(t)\,dt - k_{q,2_u-2_g}^{Rg}[Rg] \int_0^\infty I_{2_g}(t)dt + \frac{k_{R,2_g}}{k_{R,2_u}} k_{q,2_u-2_g}^{I_2(X)}[I_2(X)] \int_0^\infty I_{2_u}(t)dt - k_{q,2_u-2_g}^{I_2(X)}[I_2(X)] \int_0^\infty I_{2_g}(t)\,dt - k_{R,2_g} \int_0^\infty I_{2_g}(t)\,dt \tag{13}$$

where $I_{2_g}(t \rightarrow \infty) = I_{2_g}(t=0) = 0$. If we set $\int_0^\infty I_i(t)dt = S_i$, the ratio of the emission intensities from the 2_g ($^1D_2$) state to that from the 2_u ($^1D_2$) state, S_{2_g}/S_{2_u}, can be written as

$$\frac{S_{2_g}}{S_{2_u}} = \frac{k_{R,2_g}}{k_{R,2_u}} \frac{k_{q,2_u-2_g}^{Rg}[Rg] + k_{q,2_u-2_g}^{I_2(X)}[I_2(X)]}{k_{q,2_u-2_g}^{Rg}[Rg] + k_{q,2_u-2_g}^{I_2(X)}[I_2(X)] + k_{R,2_g}} \tag{14}$$

When the pressure of the noble gas atoms is low, $k_{q,2_u-2_g}^{Rg}[Rg] \ll k_{R,2_g}$, and by ignoring the reverse reaction in reaction 8, eq 14 can be rewritten as

$$\frac{S_{2_g}}{S_{2_u}} \simeq \frac{k_{R,2_g}}{k_{R,2_u}} \frac{k_{q,2_u-2_g}^{Rg}[Rg] + k_{q,2_u-2_g}^{I_2(X)}[I_2(X)]}{k_{q,2_u-2_g}^{I_2(X)}[I_2(X)] + k_{R,2_g}} \tag{15}$$

Here, $k_{R,2_u}$ and $k_{R,2_g}$ are the reciprocals of the collision-free fluorescence lifetimes of the 2_u ($^1D_2$) and 2_g ($^1D_2$) states, which are $k_{R,2_u} = (4.68 \pm 0.02) \times 10^7\ s^{-1}$ and $k_{R,2_g} = (2.24 \pm 0.04) \times 10^7\ s^{-1}$, respectively. $k_{q,2_u-2_g}^{I_2(X)}$ is the rate constant due to the self-quenching 2_u ($^1D_2$) – 2_g ($^1D_2$) process, which is $k_{q,2_u-2_g}^{I_2(X)} = (1.89 \pm 0.01) \times 10^{-10}$ cm^3 molecule^{-1} s^{-1} for 2_u ($^1D_2$) $v = 3$.[21] The integrated intensity ratio S_{2_g}/S_{2_u} is determined from the emission spectra under various noble gas pressures and is plotted against the number density of noble gas atoms Ar and Kr, [Rg], as shown in Figure 5. Using the slope of fitted lines in Figure 5 and the value of $[I_2(X)] = 7.56 \times 10^{15}$ molecules cm^{-3} for $p(I_2)$ = 0.2 Torr, the rate constants for $I_2(2_u)$ + Ar and $I_2(2_u)$ + Kr were determined to be $k_{q,2_u-2_g}^{Ar} = (9.61 \pm 0.63) \times 10^{-11}$ cm^3 molecule^{-1} s^{-1} and $k_{q,2_u-2_g}^{Kr} = (4.87 \pm 0.34) \times 10^{-11}$ cm^3 molecule^{-1} s^{-1}, respectively. The ratios of these values to the total collisional rate constants $k_{q,2_u}^{Rg}$ are $k_{q,2_u-2_g}^{Ar}/k_{q,2_u}^{Ar} \sim 0.21$ and $k_{q,2_u-2_g}^{Kr}/k_{q,2_u}^{Kr} \sim 0.12$, respectively. In other words, the collisional

https://doi.org/10.1021/acsomega.1c06185
ACS Omega 2022, 7, 3605−3612

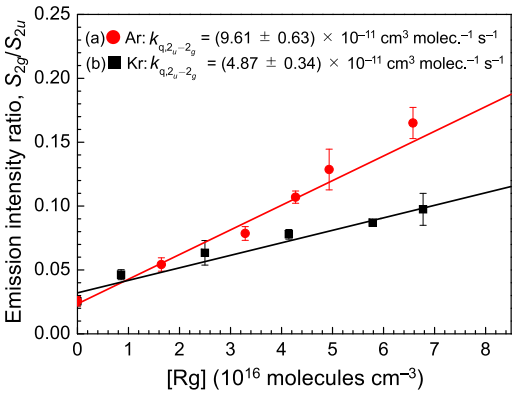

Figure 5. Ratios of the integrated emission intensity from the 2_u ($^1D_2$) state to the emission from the 2_g ($^1D_2$) state, S_{2_g}/S_{2_u}, against the quencher density, [Rg]. The self-quenching rate constants can be derived using eq 15. Quencher; red circle (a): Ar, black square (b): Kr.

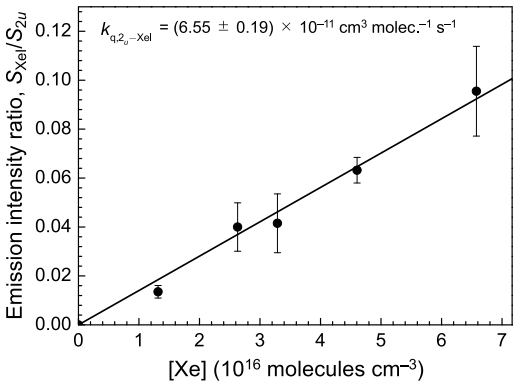

Figure 6. Ratios of the integrated emission intensity from the 2_u ($^1D_2$) state of I_2 to the emission from the B ($1/2\ ^2P_{3/2}$) state of XeI, S_{XeI}/S_{2_u}, against the Xe density, [Xe]. The reaction rate constant can be derived using eq 19.

process for the generation of the 2_g ($^1D_2$) state in reaction 8 accounts for ~21 and ~12% for Ar and Kr in the total quenching process, respectively.

2.3. Rate Constant of the Formation of XeI (B). The rate constant of the XeI (B) excimer production process 9 was then evaluated. In addition to reaction 9, the following radiative process must be considered in the rate equation

$$\mathrm{XeI}(B) \rightarrow \mathrm{XeI}(X) + h\nu\text{: } k_{\mathrm{R,XeI}} \tag{16}$$

In the present analysis, the process shown in reaction 17 is neglected because the number density of iodine molecules in the 2_g ($^1D_2$) state is much smaller than that in the 2_u ($^1D_2$) state.

$$\mathrm{I}_2(2_g) + \mathrm{Xe} \rightleftarrows \mathrm{XeI}(B) + \mathrm{I}\text{: } k^{\mathrm{Xe}}_{\mathrm{q},2_u-\mathrm{XeI}} \tag{17}$$

If we also ignore the reverse reaction in process 9, the rate equation can be written as

$$\frac{\mathrm{d}N_{\mathrm{XeI}}(t)}{\mathrm{d}t} = k^{\mathrm{Xe}}_{\mathrm{q},2_u-\mathrm{XeI}} N_{2_u}(t)[\mathrm{Xe}] - k_{\mathrm{R,XeI}} N_{\mathrm{XeI}}(t) \tag{18}$$

The integral intensity ratio S_{XeI}/S_{2_u} is obtained by integrating eq 18 as follows

$$\frac{S_{\mathrm{XeI}}}{S_{2_u}} = \frac{k^{\mathrm{Xe}}_{\mathrm{q},2_u-\mathrm{XeI}}}{k_{\mathrm{R},2_u}}[\mathrm{Xe}] \tag{19}$$

From the integrated intensity ratio S_{XeI}/S_{2_u} plotted against the number density of Xe (Figure 6), the rate constant of the formation of XeI was determined to be $k^{\mathrm{Xe}}_{\mathrm{q},2_u-\mathrm{XeI}} = (6.55 \pm 0.19) \times 10^{-11}$ cm^3 molecule^{-1} s^{-1}. The ratio of this value to the total deactivation rate by Xe was $k^{\mathrm{Xe}}_{\mathrm{q},2_u-\mathrm{XeI}}/k^{\mathrm{Xe}}_{\mathrm{q},2_u} \sim 0.096$. Thus, the collisional process 9 accounts for ~9.6% of the total quenching process 5 by the Xe atom. Table 1 summarizes the rate constants determined in this study. Self-quenching rate constants determined in past studies were also included.

2.4. Harpoon Mechanism for the Quenching Process. The quenching rate constant $k^{\mathrm{Rg}}_{\mathrm{q},2_u}$ is related to the collisional cross-section σ as follows

$$\sigma = \frac{k^{\mathrm{Rg}}_{\mathrm{q},2_u}}{c_{\mathrm{rel}}} \tag{20}$$

where c_{rel} is the average relative velocity between excited iodine molecule and noble gas atom and is expressed from the gas molecule kinetics theory as follows

$$c_{\mathrm{rel}} = \sqrt{\frac{8RT}{\pi\mu}} \tag{21}$$

In eq 21, R is the gas constant and μ is the reduced mass. The average relative velocities c_{rel} between the excited iodine molecule and Ar, Kr, and Xe are 426.1, 315.3, and 269.1 m s^{-1}, respectively, at T = 296 K. The collisional cross-section σ and collision radius R_{coll} are listed in Table 2.

It can be seen that the collisional cross sections shown in Table 2 are negatively correlated with the ionization energy of the quencher atoms and are considerably larger than the size of the excited iodine molecule and noble gas atoms. Such features indicate the harpoon mechanism to be responsible for the rapid progress of the reactions.[27]

$$\mathrm{I}_2(\mathrm{IPS}) + \mathrm{Rg} \rightarrow [\mathrm{I}_2(\mathrm{IPS})^- \cdots \mathrm{Rg}^+] \rightarrow \text{products} \tag{22}$$

The harpoon mechanism is an electron-transfer reaction that occurs over a long distance. The formation of excimer-XeI shown in the diagram in Figure 7 is one example. The curve $V_1(R)$ represents the electrically neutral potential curve between Xe and I_2, given by

$$V_1(R) = E(\mathrm{I}_2^*) - \frac{C_6}{R^6} \tag{23}$$

where $E(\mathrm{I}_2^*)$ and C_6 are the energies of the 2_u ($^1D_2$) ion-pair state and proportional constant, respectively. In addition, $V_2(R)$ represents the Coulomb potential between Xe^+ and I_2^- given as

$$V_2(R) = E(\mathrm{I}_2^*) + E_{\mathrm{ip}}(\mathrm{Rg}) - E_{\mathrm{ea}}(\mathrm{I}_2^*) - \frac{e^2}{4\pi\varepsilon_0 R} \tag{24}$$

where $E_{\mathrm{ip}}(\mathrm{Rg})$ is the ionization potential of the noble gas atoms, which is 15.8, 14.0, and 12.1 eV for Ar, Kr, and Xe, respectively.[29−31] $E_{\mathrm{ea}}(\mathrm{I}_2^*)$ is the electron affinity of excited I_2. The excited iodine molecules and noble gas atoms approach the potential curve $V_1(R)$. When the distance R between the excited iodine molecule and the noble gas atom reaches critical reaction radius, R_{harp}, the reaction proceeds along the Coulomb potential $V_2(R)$, and excimer XeI(B) is produced. The produced XeI(B) emits 253 nm fluorescence and finally dissociates into Xe and I atoms. By neglecting the term of the covalent interaction

https://doi.org/10.1021/acsomega.1c06185
ACS Omega 2022, 7, 3605−3612

Table 1. Quenching Rate Constant, k_q^Q, Rate Constant of the 2_u ($^1D_2$)−2_g ($^1D_2$) Collisional Transfer, $k_{q,2_u-2_g}^Q$, and Rate Constant of the Formation of XeI, $k_{q,2_u-XeI}^{Xe}$

quencher	k_q^Q (experimental)[a]	$k_{q,2_u-2_g}^Q$ (experimental)[a]	$k_{q,2_u-XeI}^{Xe}$ (experimental)[a]
Ar	$(4.55 \pm 0.42) \times 10^{-10}$	$(9.61 \pm 0.63) \times 10^{-11}$	
Kr	$(4.23 \pm 0.11) \times 10^{-10}$	$(4.87 \pm 0.34) \times 10^{-11}$	
Xe	$(6.83 \pm 0.16) \times 10^{-10}$		$(6.55 \pm 0.19) \times 10^{-11}$
I_2 (X)[21]	$(1.30 \pm 0.01) \times 10^{-9}$	$(1.89 \pm 0.01) \times 10^{-10}$	

[a] cm^3 $molecule^{-1}$ s^{-1}.

Table 2. Experimental and Theoretical Quenching Rate Constants, $k_{q,2_u}^{Rg}$, Collisional Cross Section σ, and Collisional Radius, R_{coll}

quencher	$k_{q,2_u}^{Rg}$ (experimental)[a]	σ[b]	R_{coll}[c]	$k_{q,2_u}^{Rg}$ (theoretical)[a]
Ar	$(4.55 \pm 0.42) \times 10^{-10}$	107 ± 10	5.84	$(4.10 \pm 0.15) \times 10^{-10}$
Kr	$(4.23 \pm 0.11) \times 10^{-10}$	134 ± 3	6.55	$(3.88 \pm 0.22) \times 10^{-10}$
Xe	$(6.83 \pm 0.16) \times 10^{-10}$	254 ± 6	9.01	$(4.91 \pm 0.68) \times 10^{-10}$

[a] cm^3 $molecule^{-1}$ s^{-1}. [b] Å^2. [c] Å.

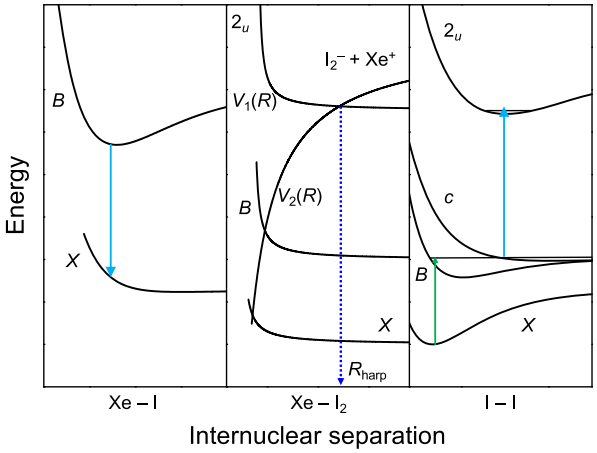

Figure 7. Schematic potential model for the harpoon mechanism. The right panel illustrates the potential energy curves of the $X\ ^1\Sigma_g^+$, $B\ ^3\Pi(0_u^+)$, $c\ ^1\Pi_g$, and 2_u ($^1D_2$) states of I_2. The central panel shows the schematic potentials of the activated complex, I_2−Xe, where $V_1(R)$ and $V_2(R)$ represent the potential energy curves of the neutral and ionic complexes, respectively. The left panel shows potentials of XeI. When the I_2 molecule in the 2_u ($^1D_2$) state approaches the Xe atom, an activated complex is formed. The complex forms an ionic pair by electron transfer at the intersection of V_1 and V_2 to produce the electronically excited B ($1/2\ ^2P_{3/2}$) state of XeI. Then, XeI (B), emitting fluorescence, relaxes to the ground state and dissociates to Xe + I ($^2P_{3/2}$).

between I_2* and Rg, the critical reaction radius is the distance between the two particles at the intersection of potentials $V_1(R)$ and $V_2(R)$ and is expressed as

$$R_{harp} = \frac{e^2}{4\pi\varepsilon_0} \frac{1}{E_{ip}(Rg) - E_{ea}(I_2^*)} \quad (25)$$

It would be of interest to compare the theoretical R_{harp} with the experimental values obtained in this study. To estimate the electron affinity $E_{ea}(I_2^*)$ of the 2_u ($^1D_2$) state, we considered the energy of the anion I_2^- state. The electronic configuration of the 2_u ($^1D_2$) state is $(\sigma_g)^2(\pi_u)^3(\pi_g^*)^3(\sigma_u^*)^2$: $^1\Delta_u$.[27,32] The electronic configurations of the anionic states are $(\sigma_g)^2(\pi_u)^4(\pi_g^*)^3(\sigma_u^*)^2$: $^2\Pi_u$ and $(\sigma_g)^2(\pi_u)^3(\pi_g^*)^4(\sigma_u^*)^2$: $^2\Pi_g$. Ab initio calculations predict that the electronic states of $^2\Pi_{g,3/2}$, $^2\Pi_{g,1/2}$, $^2\Pi_{u,3/2}$, and $^2\Pi_{u,1/2}$ are located at ∼0.8, ∼0.9, ∼0.9, and ∼1.7 eV above the ground state of the I_2^- anion, respectively.[33] Then, $E_{ea}(I_2^*)$ of the 2_u ($^1D_2$) state was estimated to be 7.6−8.5 eV. The critical reaction radius, R_{harp}, in eq 25 assumes two point-charge particles. Thus, the actual value of the collisional radius R_{coll} can be expressed as

$$R_{coll} = R_{harp} + b \quad (26)$$

where b is the impact parameter, estimated from the sum of half of the equilibrium internuclear distance of the 2_u ($^1D_2$) state, ∼1.75 Å, and the van der Waals radius of the noble gases (1.88, 2.02, and 2.16 Å for Ar, Kr, and Xe, respectively).[34] The calculated quenching rate constants are listed in Table 2 and reflect the trend of the experimental rate constants, providing a strong support for the harpoon mechanism for the collisional process in the 2_u ($^1D_2$) state.

3. CONCLUSIONS

In this work, we present a kinetic analysis of the collisional process between the 2_u ($^1D_2$) (v = 3) ion-pair state of I_2 and noble gas atoms, Ar, Kr, and Xe, as quenchers. Approximately 21 and 12% of the quenching process by Ar and Kr, respectively, were found to be energy transferred to the energetically peripheral 2_g ($^1D_2$) ion-pair state. The formation of excimer XeI(B) was observed in the collisional process with Xe, which accounted for 9.6% of the total quenching process by Xe. The collisional cross sections calculated from the quenching rate constants were considerably larger than the molecular size. The theoretical rate constants calculated from the ionization energy of the quencher atoms and the electron affinity of the 2_u ($^1D_2$) state, assuming the harpoon mechanism, reflected the trend of the experimental rate constants.

4. EXPERIMENTAL METHODS

Excitation to the single rovibronic level of the 2_u ($^1D_2$) state was performed by a perturbation-facilitated optical−optical double resonance technique through the $c\ ^1\Pi_g \sim B\ ^3\Pi(0_u^+)$ double-faced valence state as the intermediate state.[21,35] A schematic experimental setup is shown in Figure 8. Two dye lasers (Continuum ND6000) pumped by third (355 nm) and second

https://doi.org/10.1021/acsomega.1c06185
ACS Omega 2022, 7, 3605−3612

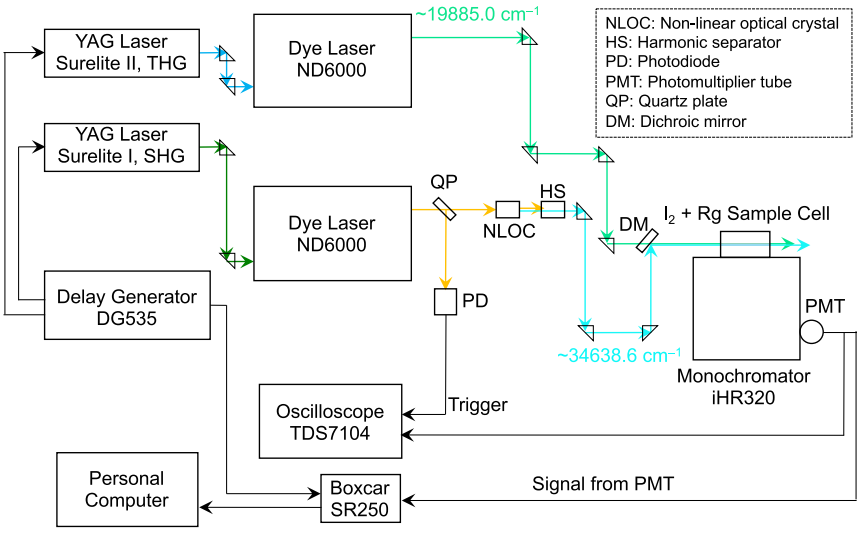

Figure 8. Schematic experimental setup.

(532 nm) harmonic outputs of Nd^{3+}:YAG lasers (Continuum Surelite I and II) were used as excitation light sources. The timing between the *Q*-switch and flash lamp of each laser was controlled by a pulse generator (Stanford Research System DG535). The output from the first dye laser (LD489, methanol solution) at ~19885.0 cm^{-1} was used as the excitation light for the $c\ ^1\Pi_g\ (v_c = 13, J_c = 23) \sim B\ ^3\Pi(0_u^+)\ (v_B = 59, J_B = 22) \leftarrow X\ ^1\Sigma_g^+$ $(v_X = 0, J_X = 23)$ transition. The second harmonic output at ~34638.6 cm^{-1} from the second dye laser (rhodamine 610 + rhodamine 590, methanol solution), frequency doubled by a KDP crystal (Inrad Optics), was employed as the excitation light for the $2_u\ (^1D_2)\ (v = 3, J = 23) \leftarrow c\ ^1\Pi_g\ (v_c = 13, J_c = 23)$ transition. Both laser beams were spatially overlapped in a quartz cell filled with vapor I_2 (~0.2 Torr) at 23 °C and noble gas atoms (Ar, Kr, and Xe). The sample cell is made of synthetic fused silica. Both entrance and exit window surfaces are perpendicular to the laser propagation direction. The pulse width of the two laser pulses was typically ~6 ns. The delay time between the two laser pulses was adjusted to 15 ns to eliminate their temporal overlap, avoiding any potential coherent process affecting the fluorescence decay profile. The sample pressure was measured using a capacitance manometer (Edwards Barocel). To minimize the effects of contamination, such as water, the sample cell was heated at a pressure of 10^{-4} Pa before sample installation. The samples were then sublimated multiple times under vacuum to remove any impurities.

To measure the dispersed fluorescence spectrum, the fluorescence from the electronically excited state of I_2 was monitored from the side window of the cell and detected by a photomultiplier tube (PMT) (Hamamatsu Photonics R928) through a monochromator (HORIBA/Jobin-Yvon iHR 320 with a grating 2400 grooves/mm). The signal from the PMT was integrated by a preamplifier (Stanford Research System SR240) and a boxcar integrator (Stanford Research System SR250) at an arbitrary number of times and then transferred to a PC via a digital multimeter (Sanwa PC5000) for later analysis. The emission spectra were recorded five times and averaged to obtain an accurate intensity ratio. The sensitivity correction of the spectroscopic system consisting of a sample cell, a monochromator, and a photomultiplier tube was performed by measuring the spectrum of a deuterium lamp (Hamamatsu Photonics L9841, MgF_2 window) with a known radiation intensity. To account for the absorption of the window of the sample quartz cell, a quartz plate of the same thickness (2 mm) as the cell window was placed between the lamp and the monochromator. By measuring the radiation spectrum of the deuterium lamp in the region of 200−380 nm and comparing it with the irradiance data supplied by the manufacturer, the instrument function was determined, and the intensity of the emission spectrum was calibrated.

The temporal profiles of the emission were observed using a fast response photomultiplier tube (Hamamatsu Photonics R2496, time response: 0.7 ns) and directly transferred to an oscilloscope (Tektronix TDS7104). The captured temporal signals were integrated approximately 3000 times (~5 min at a repetition rate of 10 Hz).

AUTHOR INFORMATION

Corresponding Authors

Shoma Hoshino − *Department of Chemistry, Faculty of Science Division I, Tokyo University of Science, Shinjuku, Tokyo 162-8601, Japan*; orcid.org/0000-0002-2476-1504; Email: shom@rs.tus.ac.jp

Oji Yamamoto − *Department of Chemistry, Faculty of Science Division I, Tokyo University of Science, Shinjuku, Tokyo 162-8601, Japan*; Email: ojiyamamoto@outlook.jp

Koichi Tsukiyama − *Department of Chemistry, Faculty of Science Division I, Tokyo University of Science, Shinjuku, Tokyo 162-8601, Japan*; Email: tsuki@rs.tus.ac.jp

Complete contact information is available at: https://pubs.acs.org/10.1021/acsomega.1c06185

Funding

This work was partly supported by JSPS KAKENHI (grant number JP20K15235).

Notes

The authors declare no competing financial interest.

REFERENCES

(1) Brand, J. C. D.; Hoy, A. R. Multiphoton Spectra and States of Halogens. *Appl. Spectrosc. Rev.* **1987**, *23*, 285−328.

(2) Alekseyev, V. A. Ion-Pair States of I_2, Br_2, IBr, and ICl. *Opt. Spektrosk.* **2005**, *99*, 719−730.

https://doi.org/10.1021/acsomega.1c06185
ACS Omega 2022, 7, 3605−3612

(3) Stuke, M.; Schäfer, F. P. Enrichment of chlorine isotopes by selective photoaddition of iodine chloride to acetylene. *Chem. Phys. Lett.* **1977**, *48*, 271−273.
(4) Stuke, M.; Marinero, E. E. Resonance in the rotational dependence of the isotope-selective reaction between $I^iCl(A\ ^3\Pi_1)$ and acetylene. *Chem. Phys. Lett.* **1979**, *68*, 28−30.
(5) Hoshino, S.; Ishiwata, T.; Nakano, Y.; Fukushima, M.; Fujiwara, H.; Araki, M.; Tsukiyama, K. Mid-Infrared Amplified Spontaneous Emission from the $f'\ 0_g^+\ (^1D_2)$ Ion-Pair State and Spectroscopic Characterization of the Shallow $0_g^+\ (ab)$ Valence State of I_2. *J. Phys. Chem. A* **2019**, *123*, 7590−7596.
(6) Hoshino, S.; Araki, M.; Nakano, Y.; Ishiwata, T.; Tsukiyama, K. Infrared radiative decay dynamics from the $\gamma\ 1_u\ (^3P_2)$, $H\ 1_u\ (^3P_1)$, and $1_u\ (^1D_2)$ ion-pair states of I_2 observed by a perturbation facilitated optical-optical double resonance technique. *J. Chem. Phys.* **2016**, *144*, 034302.
(7) Hoshino, S.; Araki, M.; Ishiwata, T.; Tsukiyama, K. Infrared amplified spontaneous emission from the $0_g^+\ (^3P_0)$ and $0_g^+\ (^1D_2)$ ion-pair states of molecular bromine. *Phys. Chem. Chem. Phys.* **2016**, *18*, 19464−19471.
(8) Hoshino, S.; Yamamoto, O.; Tsukiyama, K. Laser induced amplified spontaneous emission between the ion-pair states of Cl_2. *J. Mol. Spectrosc.* **2021**, *380*, 111513.
(9) Hoshino, S.; Abe, R.; Yamamoto, O.; Tsukiyama, K. Suppression of laser induced amplified spontaneous emission between the $f\ 0_g^+\ (^3P_0)$ and $D\ 0_u^+\ (^3P_2)$ ion-pair states of I_2. *Chem. Phys. Lett.* **2020**, *751*, 137497.
(10) Steinfeld, J. I. Rate Data for Inelastic Collision Processes in the Diatomic Halogen Molecules. *J. Phys. Chem. Ref. Data* **1984**, *13*, 445−553.
(11) Oldenberg, O. Über Elementarvorgänge bei Ausstrahlung der Jodbanden. *Z. Phys.* **1924**, *25*, 136−159.
(12) Tellinghuisen, J.; Fei, S.; Zheng, X.; Heaven, M. C. Observation and analysis of the $D' \leftarrow A'$ transition of I_2 in a free-jet expansion. *Chem. Phys. Lett.* **1991**, *176*, 373−378.
(13) Tellinghuisen, J.; Phillips, L. F. Kinetics of iodine following photolysis at 1930 Å: temperature dependence of A'-state quenching. *J. Phys. Chem.* **1986**, *90*, 5108−5120.
(14) Tscherbul, T. V.; Buchachenko, A. A.; Akopyan, M. E.; Poretsky, S. A.; Pravilov, A. M.; Stephenson, T. A. Collision-induced non-adiabatic transitions between the ion-pair states of molecular iodine: A challenge for experiment and theory. *Phys. Chem. Chem. Phys.* **2004**, *6*, 3201−3214.
(15) Ubachs, W.; Aben, I.; Milan, J. B.; Somsen, G. J.; Stuiver, A. G.; Hogervorst, W. Radiative and collisional relaxation of a single rovibrational quantum state of I_2:$E(0_g^+)$, v = 8, J = 56. *Chem. Phys.* **1993**, *174*, 285−295.
(16) Akopyan, M. E.; Bibinov, N. K.; Kokh, D. B.; Pravilov, A. M.; Stepanov, M. B.; Vasyutinskii, O. S. The 'approach-induced' $I_2\ (E\ 0_g^+ \leftrightarrow D\ 0_u^+)$ transition. *Chem. Phys.* **1999**, *242*, 263−272.
(17) Fecko, C. J.; Freedman, M. A.; Stephenson, T. A. Collision-induced electronic energy transfer from v = 0 of the $E(0_g^+)$ ion-pair state in I_2: Collisions with $I_2(X)$. *J. Chem. Phys.* **2001**, *115*, 4132−4138.
(18) Fecko, C. J.; Freedman, M. A.; Stephenson, T. A. Collision-induced electronic energy transfer from v = 0 of the $E(0_g^+)$ ion-pair state in I_2: Collisions with He and Ar. *J. Chem. Phys.* **2002**, *116*, 1361−1369.
(19) Ridley, T.; Lawley, K. P.; Donovan, R. J. Amplified spontaneous emission and collisional transfer from the $f\ 0_g^+(^3P_0)$ ion-pair state of I_2. *J. Chem. Phys.* **2009**, *130*, 124302.
(20) Akopyan, M. E.; Chinkova, I. Y.; Fedorova, T. V.; Poretsky, S. A.; Pravilov, A. M. The collision-induced non-adiabatic transitions from the $f\ 0_g^+$ state of the iodine ion-pair second tier. *Chem. Phys.* **2004**, *302*, 61−67.
(21) Hoshino, S.; Nakano, Y.; Araki, M.; Ishiwata, T.; Tsukiyama, K. Collision induced state-to-state energy transfer dynamics between the $2_u\ (^1D_2)$ and $2_g\ (^1D_2)$ ion-pair states of I_2. *J. Chem. Phys.* **2016**, *18*, 14292−14298.
(22) Akopyan, M. E.; Bibinov, N. K.; Kokh, D. B.; Pravilov, A. M.; Sharova, O. L.; Stepanov, M. B. The approach-induced $I_2\ (E\ 0_g^+ \leftrightarrow D\ 0_u^+)$ transitions, M = He, Ar, I_2, N_2, CF_4. *Chem. Phys.* **2001**, *263*, 459−470.
(23) Akopyan, M. E.; Buchachenko, A. A.; Lukashov, S. S.; Poretsky, S. A.; Pravilov, A. M.; Suleimanov, Y. V.; Torgashkova, A. S.; Tscherbul, T. V. Non-adiabatic $E \rightarrow D, D', \beta, \gamma, \delta$ transitions in the first ion-pair tier of molecular iodine induced by collisions with I_2, He, Ar, Kr, Xe. *Chem. Phys. Lett.* **2007**, *436*, 1−6.
(24) Akopyan, M. E.; Baturo, V. V.; Lukashov, S. S.; Poretsky, S. A.; Pravilov, A. M. Non-adiabatic transitions between first tier ion-pair states of I_2 induced by collisions with Ar atoms. *Chem. Phys.* **2015**, *462*, 3−11.
(25) Akopyan, M. E.; Novikova, I. Y.; Poretsky, S. A.; Pravilov, A. M.; Smolin, A. G.; Tscherbul, T. V.; Buchachenko, A. A. Collision-induced nonadiabatic transitions in the second-tier ion-pair states of iodine molecule: Experimental and theoretical study of the $I_2(f\ 0_g^+)$ collisions with rare gas atoms. *J. Chem. Phys.* **2005**, *122*, 204318.
(26) Periasamy, N. Analysis of fluorescence decay by the nonlinear least squares method. *Biophys. J.* **1988**, *54*, 961−967.
(27) Hoshino, S.; Yamamoto, O.; Abe, R.; Nishimichi, D.; Nakano, Y.; Ishiwata, T.; Tsukiyama, K. Radiative lifetimes and self-quenching rate constants of the ion-pair states of halogen molecules. *J. Quant. Spectrosc. Radiat. Transfer* **2021**, *271*, 107722.
(28) Barnes, P. N.; Kushner, M. J. Formation of XeI(B) in low pressure inductive radio frequency electric discharges sustained in mixtures of Xe and I_2. *J. Appl. Phys.* **1996**, *80*, 5593−5597.
(29) Velchev, I.; Hogervorst, W.; Ubachs, W. Precision VUV spectroscopy of Ar I at 105 nm. *J. Phys. B: At., Mol. Opt. Phys.* **1999**, *32*, L511−L516.
(30) Saloman, E. B. Energy Levels and Observed Spectral Lines of Krypton, Kr I through Kr XXXVI. *J. Phys. Chem. Ref. Data* **2007**, *36*, 215−386.
(31) Saloman, E. B. Energy Levels and Observed Spectral Lines of Xenon, Xe I through Xe LIV. *J. Phys. Chem. Ref. Data* **2004**, *33*, 765−921.
(32) Mulliken, R. S. Iodine Revisited. *J. Chem. Phys.* **1971**, *55*, 288−309.
(33) Maslen, P. E.; Faeder, J.; Parson, R. Ab initio calculations of the ground and excited states of I_2^- and ICl^-. *Chem. Phys. Lett.* **1996**, *263*, 63−72.
(34) Bondi, A. van der Waals Volumes and Radii. *J. Phys. Chem.* **1964**, *68*, 441−451.
(35) Motohiro, S.; Umakoshi, A.; Ishiwata, T. Perturbation-Facilitated Optical-Optical Double-Resonance Spectroscopy of the $1_u(^1D)$ and $2_u(^1D)$ Ion-Pair States of I_2 through the Parity Mixing Intermediate State. *J. Mol. Spectrosc.* **2001**, *208*, 213−218.

https://doi.org/10.1021/acsomega.1c06185
ACS Omega 2022, 7, 3605−3612